Journal of Catalysis 266 (2009) 228–235

Contents lists available at ScienceDirect

Journal of Catalysis

journal homepage: www.elsevier.com/locate/jcat

Remarkable support crystal phase effect in Au/FeO_x catalyzed oxidation of 1,4-butanediol to γ-butyrolactone

Jie Huang, Wei-Lin Dai *, Kangnian Fan

Shanghai Key Laboratory of Molecular Catalysis and Innovative Materials, Department of Chemistry, Fudan University, Shanghai 200433, PR China

ARTICLE INFO

Article history:
Received 28 April 2009
Revised 12 June 2009
Accepted 12 June 2009
Available online 15 July 2009

Keywords:
Gold catalyst
1,4-butanediol
γ-Butyrolactone
Support effect
Iron-oxide

ABSTRACT

Iron oxides in different crystal forms with identical particle size and morphology are employed as supports for gold catalysts. By using the oxidative dehydrogenation of 1,4-butanediol to γ-butyrolactone as the probe reaction, combined with some characterizations such as XRD, TEM, XPS, and H_2–TPR, support effect of Au/FeO_x catalysts is established in this study. Turnover frequency value follows the order $Au/Fe_3O_4 > Au/\alpha\text{-}Fe_2O_3 > Au/\gamma\text{-}Fe_2O_3$. Size effect of Au/Fe_3O_4 catalysts with different gold particle size distributions obtained by treating under different atmospheres is also studied for comparison, and the results imply the slight effect of gold particle size. Variation in catalytic behavior of gold catalysts on different iron-oxide supports originates from the discrepancy in gold geometry, gold oxidation state, and gold-support contact interface structures which are caused by difference in support intrinsic properties such as microcrystalline structure and oxidation state.

1. Introduction

Gold catalysts have been proven to be highly active in many reactions including CO oxidation [1], water gas shift (WGS) reaction [2,3], selective oxidation of alcohols [4,5], sugars [6] and alkenes [7,8], total oxidation of hydrocarbons [9], and volatile organic compounds [10], and selective hydrogenation of α,β-unsaturated ketones, aldehydes, or acetylene [11,12]. Many factors are supposed to have influence on the activity of gold catalysts, such as gold particle size [13], gold oxidation state [14], geometry of gold particles [15], moisture effect [16], and support effect [17–19]. In gold catalysts, support plays an important role by acting as the electron modifier, providing new reaction sites, or working as active species during the catalytic procedures. Support can also stabilize the active gold species by preventing them from agglomeration. In addition, it is reported that oxygen adsorption takes place on the gold-supported interface [20].

Variations in support properties bring about differences in gold particle size, geometry, and oxidation state. Therefore, it is of great importance to study the support effect. Different kinds of supports work in varied modes in gold catalysis [9,19]. According to Schubert et al., there are two types of supports in gold catalysis [17]. The first one is the inert support materials that are intrinsically less active, and small sized gold particles are essential to give high activity; the other is the reducible transition metal oxides that are able to provide reactive oxygen, and the gold particle size is not crucial in these catalysts. However, there are reports on other types of support materials such as the alkaline earth hydroxides, which require gold clusters with specific size and structure to give high activity [15]. Some non-oxide-supported gold catalysts such as $Au/LaPO_4$ [21] and Au/hydroxyapatite [22] are also active for CO oxidation. Modification or doping with a second metal oxide may decrease the gold particle size, increase the oxygen vacancies [23], and consequently promote catalytic activity [24,25] or stabilize gold particles from sintering [26]. Even for the same metal oxides, support effect is prominent. ZrO_2 in smaller particle size leads to the higher activity in CO oxidation [27], while mesoporous ZrO_2 was an active support in WGS reaction [28]. For $Au/\gamma\text{-}Al_2O_3$ catalysts, difference in surface structure causes variation in gold step/edge sites [29]. Shape and crystal plane of CeO_2 are crucial to the activity of Au/CeO_2 in CO oxidation reaction [30]. The crystalline type of the support is another important factor, i.e., for Au/TiO_2 catalysts the gold crystal structure depends on the TiO_2 polymorphs [31]. The Au/anatase catalyst was considered to exhibit the highest activity [32,33], while Au/brookite catalyst was the most stable [34]. Li et al. also reported that the monoclinic ZrO_2-supported gold catalyst is more active than gold on tetragonal ZrO_2 [35].

In our previous work, it was found that the structural characters of iron oxides have great influence on the activity of gold catalysts in the oxidative dehydrogenation of α,ω-diols to the corresponding lactones [36]. However, the supports used were different not only in crystal phase, but also in particle size and morphology, all of which may lead to deviation in catalytic behavior. It is essential to figure out whether it is the intrinsic nature of the iron oxide or the oxide morphology or particle size that contributes to the

* Corresponding author. Fax: +86 21 55665672.
E-mail address: wldai@fudan.edu.cn (W.-L. Dai).

0021-9517/$ - see front matter © 2009 Elsevier Inc. All rights reserved.
doi:10.1016/j.jcat.2009.06.011

high activity in the reaction. In the present study, iron oxides in different crystal phases (α-Fe_2O_3, γ-Fe_2O_3, and Fe_3O_4) are used as support materials. The iron oxides are obtained from commercial source which are prepared from the same method of identical morphology and particle size, so that the effect of iron-oxide polymorphs can be divided from the others such as the influence of iron-oxide particle size, morphology, or porosity. Among the three iron oxides, hematite (α-Fe_2O_3) holds a corundum structure with iron atoms occupying 2/3 of the octahedral cavities of the hexagonal close packed oxygen, whereas maghemite (γ-Fe_2O_3) and magnetite (Fe_3O_4) show the inverse spinel structure. In magnetite, Fe^{2+} ions occupy octahedral sites and Fe^{3+} ions are distributed evenly over octahedral and tetrahedral sites of the cubic close packed oxygen sub-lattice. In maghemite (γ-Fe_2O_3), the Fe^{2+} ions in the octahedral sites are replaced with vacancies and Fe^{3+} ions. Au/Fe_3O_4 catalysts with different gold particle size obtained by treating under different atmospheres are also investigated for comparison to make clear whether the size effect or the support effect is more important.

Behavior of gold catalysts in liquid phase reactions differs from that in gas phase reactions. Thus it is of vital importance to study the support effect in liquid phase oxidations considering that there are few reports on the support effect of gold catalysts in alcohol oxidation. The oxidative dehydrogenation of 1,4-butanediol to γ-butyrolactone is employed as a probe reaction in this study. Lactones and their derivatives are widely distributed in nature, and can be used as solvent [37], extraction agent, and intermediate of many biomedical products, fibers and pesticides [38]. Hence they get wide applications in agriculture, petroleum industry, pharmaceutics, and in synthesis of resins and fibers. Herein we provided a green and mild synthetic route of γ-butyrolactone from the oxidative dehydrogenation of 1,4-butanediol with air as oxidant and Au/FeO_x as an efficient catalyst. This novel process can avoid the utilization of fierce reaction conditions and oxidants, and meet the demands of green chemistry.

2. Experimental

2.1. Catalyst preparation

The commercial FeO_x (α-Fe_2O_3, γ-Fe_2O_3, and Fe_3O_4) are purchased from Fangyuan Nano Material Institute of Anhui University of Technology in China. All the samples are used as gold catalyst supports without any further pretreatment. Deposition of gold onto the FeO_x substrate is carried out using the homogeneous deposition–precipitation method by using urea as precipitation agent. 10 ml of $HAuCl_4$ aqueous solution (2.43×10^{-3} mol L^{-1}) is added into 50 ml of deionized water, followed by the addition of 2.92 g of urea. 0.6 g of FeO_x is then added into the above solution. The mixture is kept stirring for 2 h at 353 K. The as-prepared precipitates are collected by filtration, washed three times with deionized water, and dried in air overnight at 373 K, and then calcined in air for 4 h at 573 K.

Reduction of the catalysts with hydrogen flow and thermal treatment in argon flow are carried out in a tube furnace with the flow rate of 60 ml min^{-1} under ambient pressure in 5% H_2-Ar mixture or pure argon at 473 and 573 K for 4 h. Because reduction at 573 K with 5% H_2-Ar leads to much larger gold particle size and poor activity, we chose 473 K as the reduction temperature according to the TPR and activity results.

2.2. Characterization

Specific surface areas of the samples are measured by nitrogen adsorption at 77 K (Micromeritics Tristar ASAP 3000) using Brunauer–Emmett–Teller (BET) method. The gold loadings are determined by the inductively coupled plasma method (ICP, thermo E.IRIS). X-ray diffraction (XRD) patterns are recorded on a Bruker D8 advance spectrometer with Cu-Kα radiation (λ = 0.154 nm), operated at 40 mA and 40 kV. Transmission electronic microscopy (TEM) is performed on a JEOL JEM 2010 transmission electron microscope. The average size of Au particles and their distributions are estimated by counting more than 300 Au particles. X-ray photoelectron spectra (XPS) are recorded under ultra high vacuum ($<10^{-6}$ Pa) at a pass energy of 93.90 eV on a Perkin Elmer PHI 5000C ESCA system by using Mg-Kα (1253.6 eV) anode. All binding energies are calibrated by using contaminant carbon (C1s = 284.6 eV). Temperature programmed reduction with hydrogen (H_2–TPR) of the samples is carried out in a full automatic XQ TP-5080 instrument (Tianjin Xianquan Co. Ltd.). About 50 mg of catalyst is packed into a reactor with quartz tubing, and pretreated with high purity argon flow at 313 K for 2 h. Reduction is carried out under a mixture of hydrogen and argon (5% H_2) at a flow rate of 20 ml min^{-1}. The temperature was linearly raised at a ramping rate of 10 K min^{-1} up to 973 K.

2.3. Activity measurements

The activity tests are carried out at 413 K in a stainless steel autoclave equipped with magnetic stirrer. In a typical run of reaction, 1.4 g of 1,4-butanediol is dissolved in 20 ml of tributyl phosphate (TBP), followed by adding 0.190 g of Au/FeO_x catalyst. Then the autoclave is sealed and 1.25 MPa air is filled. Reaction is initiated by vigorous stirring. Rate of magnetic stirring is set at 800 rpm. The reaction mixture is sampled at regular time intervals and analyzed by gas chromatography to determine the conversion and selectivity. Gas chromatography-mass spectrometer is utilized to determine the product.

3. Results

3.1. Properties of iron-oxide supports

As shown in Table 1 and Fig. 1, although they are different in crystal phases, all the supports are similar in physico-chemical properties. Iron-oxide supports, including α-Fe_2O_3, γ-Fe_2O_3, and Fe_3O_4, are in pure crystal phases as evidenced by the XRD patterns. The average particle size calculated from XRD patterns by Scherrer equation is 21, 12, and 10 nm for α-Fe_2O_3, γ-Fe_2O_3, and Fe_3O_4, respectively. Although the specific surface area of α-Fe_2O_3 is a little smaller, it is generally considered that the surface area is not a critical factor in gold catalysts in the range from 30 to 100 m^2/g [39,40]. Support effect is significant in gold catalysts, and in our previous study, it was found that gold catalysts on iron oxides with

Table 1
The physico-chemical properties and catalytic activities of Au/FeO_x catalysts.

Sample	S_{BET} (m^2/g)	Au (wt%)	D_{FeO_x}[a] (nm)	D_{Au}[b] (nm)	TOF[c] (h^{-1})
α-Fe_2O_3	40.1	0	21	–	
Au/α-Fe_2O_3	33.2	6.1	23	5.5	207
γ-Fe_2O_3	78.7	0	12	–	
Au/γ-Fe_2O_3	67.5	6.1	13	6.7	74
Fe_3O_4	77.9	0	10	–	
Au/Fe_3O_4–Ar	73.1	7.7	12	4.7	230
Au/Fe_3O_4–air	72.0	7.5	12	12[a]	122
Au/Fe_3O_4–H_2	41.4	7.3	12	2.7	153

[a] Particle size is calculated by Scherrer equation from the XRD result.
[b] Au particle size is determined by TEM. More than 300 particles are counted to give the average particle size.
[c] TOF value was calculated as mol alcohol reacted in the initial 1 h on per mol surface gold calculated from the gold dispersion.

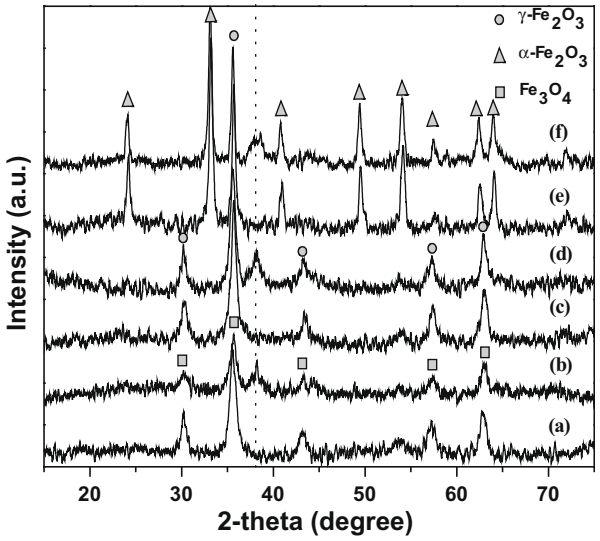

Fig. 1. XRD patterns of (a) Fe_3O_4; (b) Au/Fe_3O_4; (c) γ-Fe_2O_3; (d) Au/γ-Fe_2O_3; (e) α-Fe_2O_3; and (f) Au/α-Fe_2O_3.

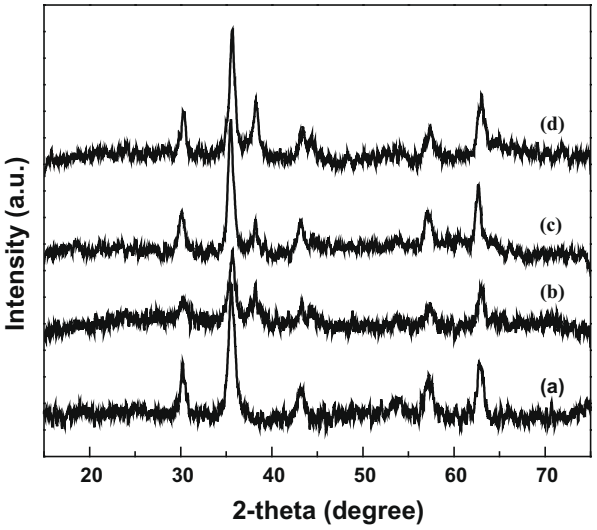

Fig. 2. XRD patterns of (a) Fe_3O_4; (b) Au/Fe_3O_4–Ar; (c) Au/Fe_3O_4–H_2; (d) Au/Fe_3O_4–air.

different morphologies and crystal phases varied greatly in catalytic behavior in the oxidation of α,ω-diols [36]. However, we are not sure whether it was caused by the morphology change or crystal evolution. Thus, to rule out other effects and to focus on the support crystal phase effect, the supports used are obtained from commercial source with similar particle size and morphology as evidenced by the above characterizations.

3.2. Morphology and crystalline structure of iron oxide-supported gold catalysts

Gold catalysts on different supports are of equal gold loading and prepared under the same conditions except for Au/Fe_3O_4 which is pretreated in argon, since calcination in air may lead to the oxidation of Fe_3O_4. Au/Fe_3O_4 catalysts treated under different conditions are also prepared for comparison. Physico-chemical properties of the as-prepared catalysts are listed in Table 1. There is a slight drop in surface area after deposition of gold in all catalysts except for Au/Fe_3O_4–H_2, of which the surface area drops from 77.9 to 41.4 m^2/g. Gold loadings determined by ICP are almost the same, and near the nominal amount (8%). It should be noted that a gold loading of 6–8% is necessary for the conversion of diols to lactones due to the difficult mass-transfer and poor selectivity if lower loading was afforded (<5%) [36]. It is found that α-Fe_2O_3 and γ-Fe_2O_3 keep their crystalline phases and particle size after deposition of gold as indicated by the XRD results (Fig. 1). As for Au/Fe_3O_4, it is not sure whether Fe_3O_4 is oxidized to γ-Fe_2O_3 or not, because both γ-Fe_2O_3 and Fe_3O_4 show inverse spinel structure and the 2θ values are quite close to each other. Appearance of the broad diffraction line at $2\theta = 38.2°$ (Au(1 1 1)) indicates the formation of small metallic gold particles in Au/ Fe_3O_4. Among catalysts on different iron oxides, Au(1 1 1) line at $2\theta = 38.2°$ in Au/γ-Fe_2O_3 is the sharpest and strongest, implying the formation of the largest gold particles. Intensity of gold diffraction line follows the trend of Au/Fe_3O_4–Ar < Au/α-Fe_2O_3 < Au/γ-Fe_2O_3, suggesting the gold particle size in the same order, which is also confirmed by the TEM results. For Au/Fe_3O_4 catalysts treated under different atmospheres, Au/Fe_3O_4–air shows the strongest gold diffraction lines (Fig. 2), with the largest average gold particle size of 12 nm, while weaker and broader lines are observed on Au/Fe_3O_4–Ar and Au/Fe_3O_4–H_2. The reasons will be discussed intensively at a later point.

Moreover, the TEM results indicated different gold particle size and size distributions of catalysts on different iron-oxide supports (Fig. 3). All the iron oxides are composed of particles with diameter ranging from 10 to 40 nm. In Au/α-Fe_2O_3, gold particles are evenly distributed on the surface of α-Fe_2O_3, with diameter ranging from 2–12 nm, and the average gold particle size is 5.5 nm. While on γ-Fe_2O_3, gold particles are relatively larger, and there are aggregated gold particles with diameter up to 14 nm. The average gold particle size increases to 6.7 nm with a larger deviation. However, there are still some gold particles smaller than 2 nm. In addition, gold density is much lower when compared to other samples, as shown in Fig. 3c, which presents only a few gold particles in the image. Small gold particles and narrow gold particle size distribution are observed on Au/Fe_3O_4–Ar, of which the average gold particle size is 4.7 nm. Pretreatment condition has strong influence on the gold particle size distribution, and as shown in Fig. 3e–h, the hydrogen pretreated Au/Fe_3O_4 catalyst (Au/Fe_3O_4–H_2) gives the smallest gold particles and the most uniform size distribution. Gold particle size ranges from 0.8 to 8 nm with average diameter of 2.7 nm, which is quite small compared to that of Au/Fe_3O_4–Ar (4.7 nm) and Au/Fe_3O_4–air (12 nm). Because of its small gold particle size, the surface density of gold particles is much higher, as shown in Fig. 3g that there are much more particles in this image compared with those of the other catalysts.

3.3. Surface content and chemical state of the Au/iron-oxide catalysts

Surface gold content and electronic state of the catalysts were characterized by XPS and the results are given in Table 2 and Figs. 4–6. It is found that gold is in the metallic form in Au/Fe_3O_4–H_2, and there is quite little oxidized gold ($Au^{\delta+}$) in Au/γ-Fe_2O_3, Au/Fe_3O_4–Ar, and Au/Fe_3O_4–air with almost same amount (about 15%), according to the deconvolution of Au 4f species. In Au/α-Fe_2O_3, more than half of the surface gold is in the oxidized state due to the stabilization of $Au^{\delta+}$ by α-Fe_2O_3. There is no charge transfer from support to gold detected in Au/Fe_3O_4-H_2, of which the Au 4f XPS peak is quite symmetric and narrow, indicating that most of the gold is metallic, or the amount of $Au^{\delta+}$ is so small that it cannot be distinguished from the background. Binding energies of Au(0) $4f_{7/2}$ were 83.0, 83.4, and 83.5 eV for Au/α-Fe_2O_3, Au/γ-Fe_2O_3, and Au/Fe_3O_4-Ar, respectively. The value is a little lower than that of bulk gold at 84.0 eV, indicating the formation of gold-support

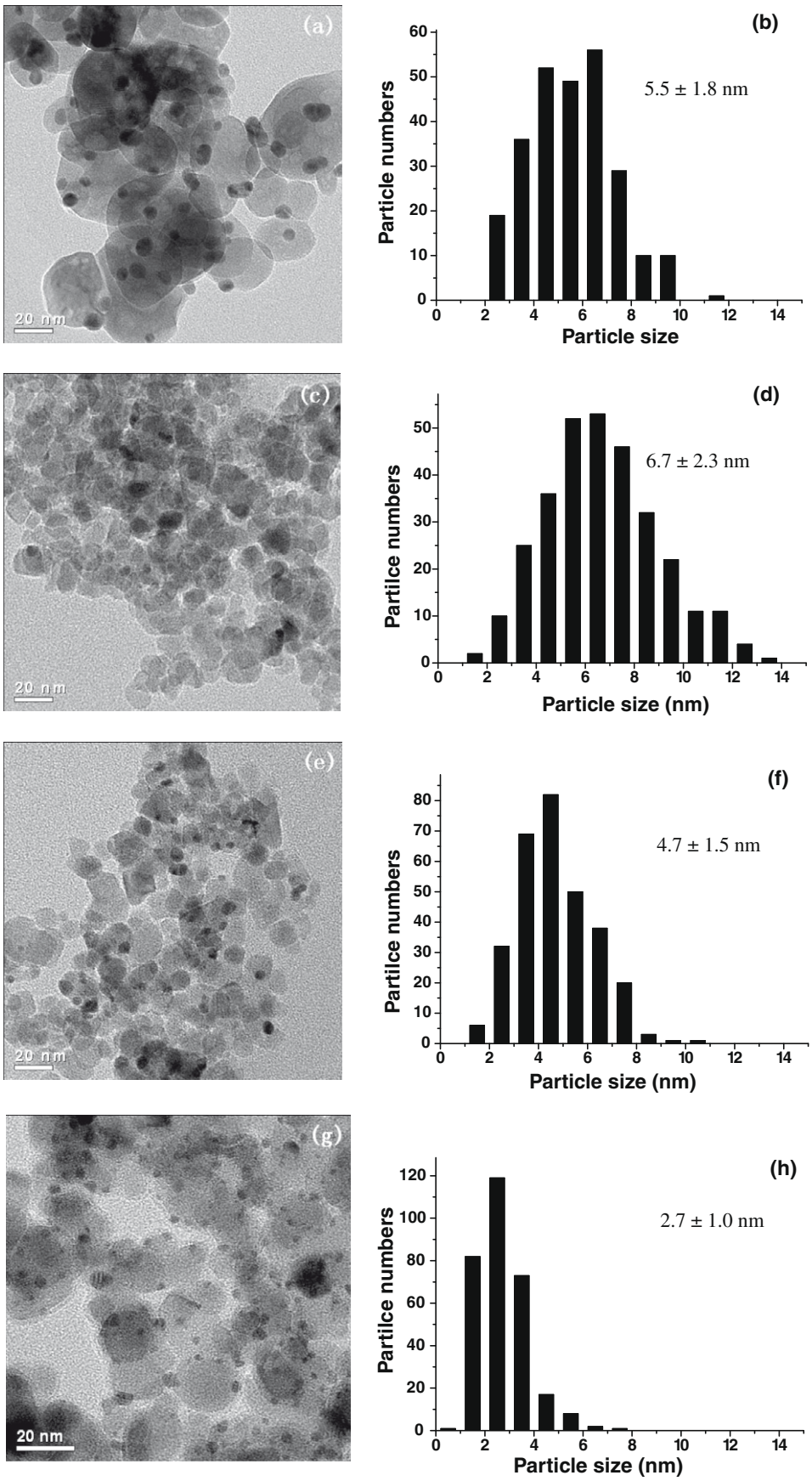

Fig. 3. TEM images and particle size distributions of Au/α-Fe_2O_3 (a,b), Au/γ-Fe_2O_3 (c,d), Au/Fe_3O_4 (e,f), and Au/Fe_3O_4–H_2 (g,h).

Table 2
Surface content and relative surface distribution of gold species of Au/FeO_x catalysts.

Sample	Au_{surf}[a] (%)	Binding energy (eV)	FWHM (eV)	Au species (%)
Au/α-Fe_2O_3	12.6	83.0	2.1	Au^0 (46)
		84.5	2.1	$Au^{\delta+}$ (54)
Au/γ-Fe_2O_3	7.6	83.4	2.1	Au^0 (84)
		84.4	2.0	$Au^{\delta+}$ (16)
Au/Fe_3O_4–Ar	6.3	83.5	2.1	Au^0 (85)
		84.3	2.0	$Au^{\delta+}$ (15)
Au/Fe_3O_4–air	6.2	83.6	2.0	Au^0 (84)
		84.7	2.0	$Au^{\delta+}$ (16)
Au/Fe_3O_4–H_2	11.3	83.5	2.2	Au^0 (100)

[a] The surface gold weight content is calculated from the ratio of Au:Fe_2O_3 obtained from the surface composition by XPS.

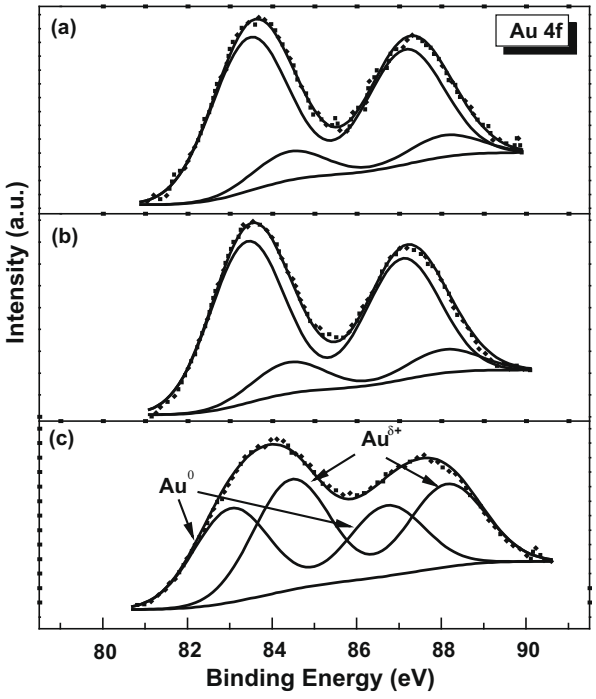

Fig. 4. Au 4f XPS spectra of (a) Au/Fe_3O_4; (b) Au/γ-Fe_2O_3; and (c) Au/α-Fe_2O_3.

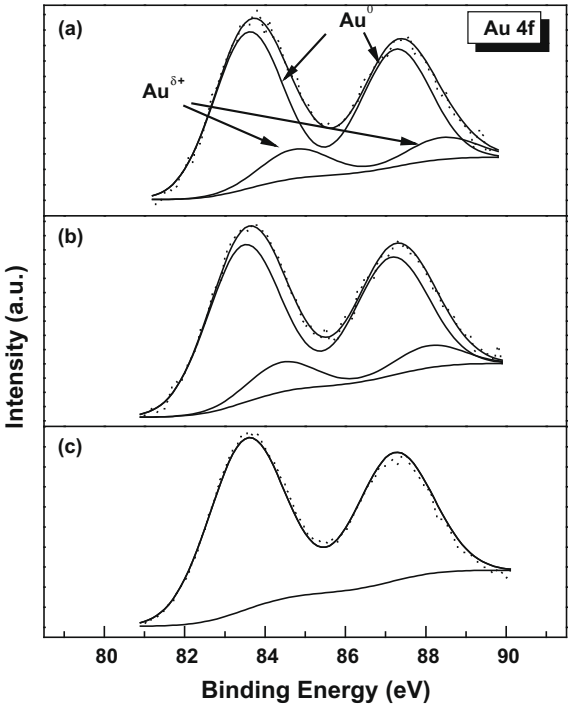

Fig. 5. Au 4f XPS spectra of (a) Au/Fe_3O_4–air; (b) Au/Fe_3O_4–Ar; and (c) Au/Fe_3O_4–H_2.

interaction. It is also found that Au/α-Fe_2O_3 has the highest gold surface content while surface gold content of Au/γ-Fe_2O_3 and Au/Fe_3O_4–Ar is near the nominal gold loading (8%). Au/Fe_3O_4–H_2 shows higher surface gold content (11.3%) than Au/Fe_3O_4–air (6.2%) and Au/Fe_3O_4–Ar (6.3%).

Fe 2p XPS peaks of the Au/Fe_3O_4 catalysts are shown in Fig. 6. There is a satellite peak at 718.9 eV beside the main peak of Fe $2p_{3/2}$ at 710.9 eV in Au/Fe_3O_4–air, which is absent in Au/Fe_3O_4–Ar and Au/Fe_3O_4–H_2. According to the literature [41], appearance of such peak is due to the oxidation of Fe_3O_4 to γ-Fe_2O_3, and thus it can be concluded that Fe_3O_4 is oxidized when calcined in air. The XPS results provided evidence of the transformation of Fe_3O_4 to γ-Fe_2O_3 which was not observed in the XRD results because of the similarity of the diffraction lines of Fe_3O_4 and γ-Fe_2O_3.

3.4. TPR behavior of the Au/iron-oxide catalysts

Addition of gold lowers the reduction temperature of Fe_2O_3 to Fe_3O_4 and leads to the difference in the shape of the reduction peak as presented in the H_2—TPR curves shown in Figs. 7 and 8. Reduction peaks at 659 and 655 K for α-Fe_2O_3 and γ-Fe_2O_3 are due to the reduction of Fe(III) to Fe_3O_4. There is a peak at 635 K for Fe_3O_4, area of which is much smaller than that of α-Fe_2O_3 and γ-Fe_2O_3. The

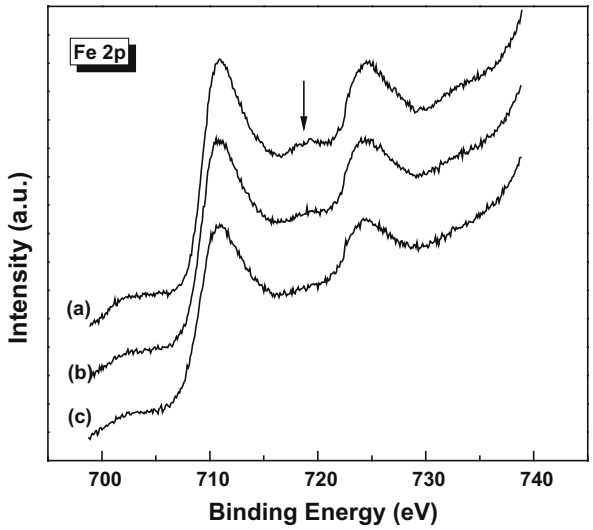

Fig. 6. Fe 2p XPS spectra of (a) Au/Fe_3O_4–air; (b) Au/Fe_3O_4–Ar; and (c) Au/Fe_3O_4–H_2.

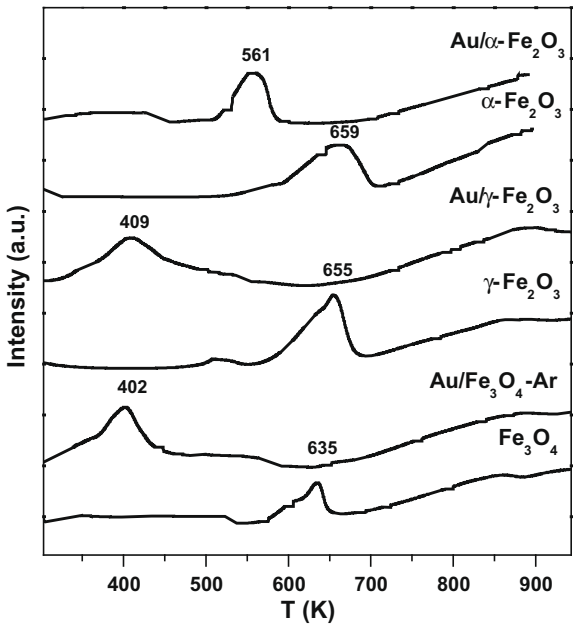

Fig. 7. H_2–TPR profiles of iron oxides and the gold catalysts on different FeO_x supports.

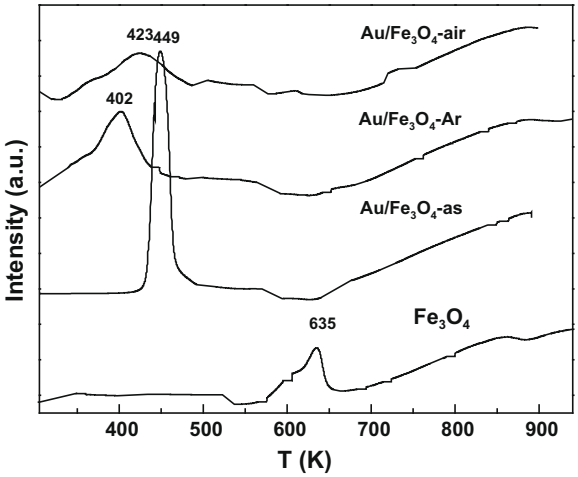

Fig. 8. H_2–TPR profiles of Fe_3O_4 and Au/Fe_3O_4 treated under different atmospheres.

peak is attributed to the reduction of the partially oxidized surface ferric hydroxide species that are formed by interaction between Fe_3O_4 and some adsorbed oxygen species and hydroxyl groups. This assumption is manifested by the lower reduction temperature (635 K) and weaker peak intensity of Fe_3O_4 than those of α-Fe_2O_3 and γ-Fe_2O_3, indicating that oxidation is not complete and these species are much easier to be reduced. Fe_3O_4 used here is small in particle size (10–20 nm in diameter), and thus when exposed to air, the adsorbed O_2 and water may cause partial oxidation of Fe_3O_4 to γ-Fe_2O_3 or some kind of ferric hydroxides. The broad reduction peak in all these samples at temperature higher than 850 K is attributed to the reduction of Fe_3O_4 to FeO and the subsequent reduction to Fe. Since all the samples are calcined before use, no reduction of gold species is observed.

Reduction peak of Fe_2O_3 to Fe_3O_4 in Au/α-Fe_2O_3 shifts to 561 K, about 100 K lower than that of pure α-Fe_2O_3. No reduction of gold is observed, in contrast to the XPS result of Au/α-Fe_2O_3. Since XPS is a surface sensitive technique that only presents surface properties, the oxidized gold species may exist only on the surface of hematite holding a small amount of the total loading so that the reduction of these species could not be detected by the H_2–TPR technique for bulk species. Reduction of Au/γ-Fe_2O_3 and Au/Fe_3O_4 occurs at even lower temperature, only 409 and 402 K for Au/γ-Fe_2O_3 and Au/Fe_3O_4–Ar. According to the above discussion and the fact that there is no other peaks at temperature range from 300 to 800 K, reduction peak around 400 K is ascribed to the reduction of Fe(III) to Fe_3O_4. Unlike the symmetric and narrow peak in Au/α-Fe_2O_3, the reduction peak widens in Au/Fe_3O_4–Ar and Au/γ-Fe_2O_3. Reduction ranges from 310 K to 520 K in Au/γ-Fe_2O_3 and from 310 to 450 K in Au/Fe_3O_4–Ar. From the above results it can be concluded that the catalysts vary in reduction behavior, and that Fe_3O_4 and γ-Fe_2O_3 exhibit higher oxygen mobility than α-Fe_2O_3 due to the more significant decrease in reduction temperature.

For Au/Fe_3O_4 calcined in argon and air flow, the negative shift of the TPR reduction peak is also observed as shown in Fig. 8. Reduction temperature of Au/Fe_3O_4–Ar is a little lower than that of Au/Fe_3O_4–air, which may be assigned to the stronger interaction between the smaller gold particles and Fe_3O_4 in Au/Fe_3O_4–Ar. H_2–TPR experiment of the as-prepared Au/Fe_3O_4 without any treatments (Au/Fe_3O_4-as) is also carried out for comparison. Reduction of Au/Fe_3O_4-as is complete below 470 K, which is lower than the pretreatment temperature of Au/Fe_3O_4–H_2 at 473 K, indicating that gold species are all reduced by treating in H_2 at 473 K. There is only one strong peak with a shoulder at the high temperature region (about 470 K) in Au/Fe_3O_4-as, and no other peaks are observed below 700 K. Strong intensity of the peak and the appearance of a shoulder peak may be formed by the overlapping of the reduction of gold and iron oxide. Therefore, it is concluded that iron oxide is also in the reduced form in Au/Fe_3O_4–H_2. Since gold is still in the oxidized form in Au/Fe_3O_4-as, the gold-support interaction is not as strong as that in Au/Fe_3O_4–Ar and Au/Fe_3O_4–air, and thus reduction temperature of Au/Fe_3O_4-as is a little higher than that of the other two catalysts. Deposition of gold or variation in support does not cause any change to high temperature TPR reduction peaks of Fe_3O_4 to FeO and Fe in all the Au/iron-oxide catalysts.

3.5. Catalytic activity of Au/FeO_x catalysts

Catalytic activity results of the Au/FeO_x catalysts in the oxidative dehydrogenation of 1,4-butanediol to γ-butyrolactone are given in Table 3, Figs. 9 and 10. After 8 h reaction at 413 K, Au/α-Fe_2O_3 shows the highest conversion and yield. 1,4-butanediol is fully consumed, and selectivity reaches 86%. Au/γ-Fe_2O_3 and Au/Fe_3O_4–Ar give the conversion of 78% and 84%, respectively. For catalysts supported on different iron oxides, both conversion and yield follow the order Au/α-Fe_2O_3 > Au/Fe_3O_4–Ar > Au/γ-Fe_2O_3. Pretreatment condition is also critical, and the catalytic activity follows the order Au/Fe_3O_4–H_2 > Au/Fe_3O_4–Ar > Au/Fe_3O_4–air. Catalytic activity of Au/Fe_3O_4–H_2 is the highest and the conversion and selectivity reaches 84% and 71%, respectively.

Table 3
Catalytic activity of Au/FeO_x catalysts in the oxidative dehydrogenation of 1,4-butanediol to γ-butyrolactone.[a]

Catalyst	Conversion (%)	Selectivity (%)
Au/α-Fe_2O_3	100	86
Au/γ-Fe_2O_3	78	69
Au/Fe_3O_4–Ar	84	65
Au/Fe_3O_4–air	69	59
Au/Fe_3O_4–H_2	84	71

[a] Reaction conditions: 0.190 g catalyst, 1.4 g 1,4-butanediol, 20 ml TBP, 1.25 Mpa air, 413 K, 8 h.

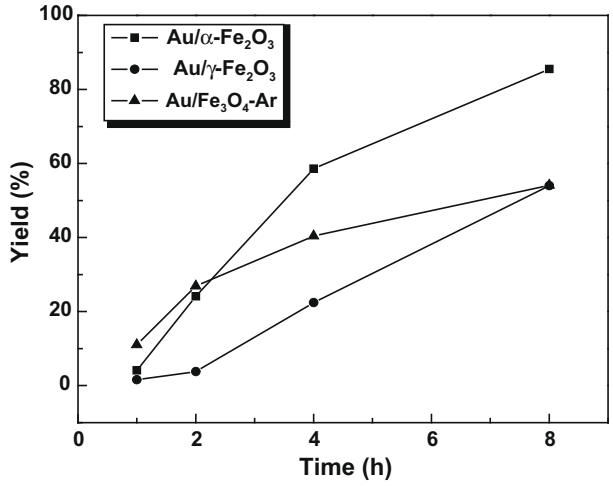

Fig. 9. Time course of oxidative dehydrogenation of 1,4-butanediol catalyzed by Au/FeO_x catalysts. Reaction conditions: 0.190 g catalyst, 1.4 g 1,4-butanediol, 20 ml TBP, 1.25 Mpa air, 413 K.

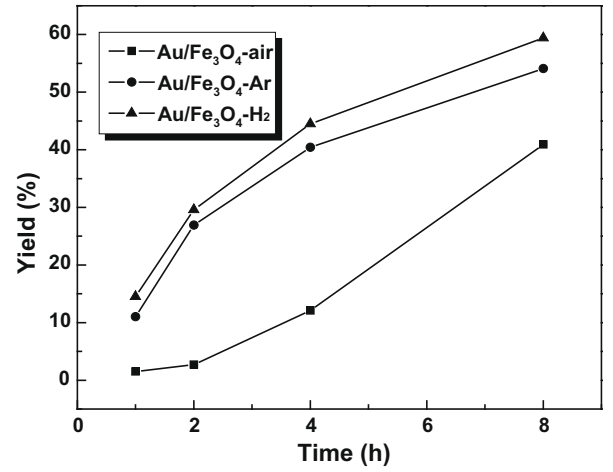

Fig. 10. Time course of oxidative dehydrogenation of 1,4-butanediol catalyzed by Au/Fe_3O_4 catalysts treated under different atmospheres. Reaction conditions: 0.190 g catalyst, 1.4 g 1,4-butanediol, 20 ml TBP, 1.25 Mpa air, 413 K.

Au/Fe_3O_4–air shows the lowest activity and only 41% yield of γ-butyrolactone is obtained. However, the turnover frequency (TOF) values of the catalysts calculated from the conversion in the initial 1 h based on per mole of surface gold do not follow the same trend. From Figs. 9 and 10, it can be seen that although the yield increases as the time prolongs, the increasing rate decreases with time. It is also found that 1,4-butanediol reacts fast at the beginning when catalyzed by Au/Fe_3O_4–Ar and Au/Fe_3O_4–H_2, whereas the reaction rate drops as time goes on, and thus the conversion and yield are lower than those over Au/α-Fe_2O_3.

4. Discussion

The present work reveals that both the support crystal phase and pretreatment atmosphere have significant influence on the size and size distributions of gold particles, gold structures, gold electronic nature, and gold-support interaction, and thus the catalytic activity. Pretreatment atmosphere mainly affects the gold particle size. Of the Au/Fe_3O_4 catalysts treated under different atmospheres, the highest γ-butyrolactone yield is obtained on Au/Fe_3O_4–H_2 that owns the smallest gold particles with the average size of 2.7 nm, and then Au/Fe_3O_4–Ar with the medium gold particle size, and finally Au/Fe_3O_4–air, with average gold particle size as large as 12 nm. However, the TOF value of Au/Fe_3O_4–H_2 is lower than that of Au/Fe_3O_4–Ar, indicating that the higher reaction rate of Au/Fe_3O_4–H_2 is due to the higher gold dispersion caused by the reduction in gold particle size. This finding coincides well with our previous results [42]. In addition, large gold particles in Au/Fe_3O_4–air are formed during the oxidation of Fe_3O_4 to γ-Fe_2O_3 under oxidative atmosphere. The low activity of Au/Fe_3O_4–air is partly due to the large gold particle size, and on the other hand is caused by the crystal phase transformation of the support from Fe_3O_4 to the less active γ-Fe_2O_3. According to the activity results in the above section, Au/γ-Fe_2O_3 presents the lowest activity among the gold catalysts supported on different iron oxides. Although the gold particle size is a little larger in γ-Fe_2O_3, increment in particle size from 4.7 to 6.3 nm could not cause such significant decrease in TOF value and γ-butyrolactone yield. As stated above, particle size is not the decisive factor because decrease in gold particle size only increases the amount of surface gold, and therefore, we infer that the support effect is the major factor.

Unlike Au/Fe_3O_4 catalysts treated under different atmospheres which show the same trend in the evolution of yield with reaction time, Au/α-Fe_2O_3, Au/γ-Fe_2O_3, and Au/Fe_3O_4–Ar own quite different time course of the reaction. Au/Fe_3O_4–Ar shows the highest initial reaction rate, with 33.1% conversion and 11.0% yield after reaction for the first hour. While Au/α-Fe_2O_3 gives the highest final conversion and yield as 100% and 85.5%, respectively, after reaction for 8 h. The lower final conversion and yield of Au/Fe_3O_4 is due to the drop in reaction rate which is caused by deactivation of the catalyst. In the oxidative reaction conditions, Fe_3O_4 support can be oxidized to the more inert γ-Fe_2O_3. For Au/γ-Fe_2O_3, reaction follows a more linear trend with lower reaction rate. It is also worth noting that the reaction course curve of Au/Fe_3O_4–air is very similar to that of Au/γ-Fe_2O_3, and according to the above results, Fe_3O_4 is partially oxidized when calcined in air. Therefore, it is the consequent formation of γ-Fe_2O_3 after calcination that causes the lower activity and the similar catalytic behavior of Au/Fe_3O_4–air to Au/γ-Fe_2O_3. From the above results, it is concluded that the changes in activity are due to the variation in intrinsic properties of the iron-oxide support, or the consequent differences in gold structure.

For supports with various crystal phases, their oxide structures, acidic/basic properties, and the surface hydroxyl group concentration [33] are different, and as a result the adsorption ability and oxygen mobility are different. There are reports of iron oxides-supported gold catalysts with different iron-oxide structures showing different catalytic behavior in the hydrogenation of α,β-unsaturated ketones [11,43]. According to these results, the activity was in the order Au/FeO(OH) > Au/iron oxy-hydroxide > Au/γ-Fe_2O_3 > Au/α-Fe_2O_3. However, reaction mechanism and support effect in gold catalysis vary with reactions. It is generally considered that lattice oxygen plays an important role in the alcohol oxidation, and the reaction undergoes the Mars-van Krevelen process. Gold increases the oxygen mobility and lattice oxygen accessibility of iron oxides, and as a result decreases the reduction temperature of Fe(III). According to the literature results, the decrease in reduction temperature of the support is due to the weakening of Fe–O bond by gold [44], reduction of Fe(III) species catalyzed by gold or hydrogen spillover from gold to support [45]. Although it is still unclear what kind of effect is dominant, there must be some kind of interactions between gold and the support. It is generally accepted that the lower reduction temperature was an indication for the stronger gold-support interaction over the same support. However, supports used in our work are different in crystal type, and the interaction would not be all the same in the three kinds of the support (as confirmed by the XPS results that the charge transfer properties differed). It is observed from the H_2–TPR results

that the shape and symmetry of the reduction peaks are quite different. This observation may be caused by the difference in geometry of gold particles or the gold-support contact interface structures that originate from difference in iron-oxide crystal phases, and are very important in the activity of gold catalysts. Differences in the nature of the support also influence kind and amount of gold species. Subnanometer gold particles in large number but low content due to their very small size (<1 nm) may play a vital role in the catalytic activity of the gold catalysts according to Herzing et al. [46].

The proposed alcohol oxidation mechanism is regarded to include the formation of alcoholate in the first step, followed by the hydride shift, and the final reoxidation process to continue the catalytic cycle. However, the adsorption process and activation of gold are unclear yet. Factors mentioned above originated from the diversity in iron-oxide crystal phases may have influence on the catalytic procedure and lead to the difference in activity of gold catalysts. Although it is not stated here, support morphology also contributes to the activity of gold catalysts, as indicated by comparison with our previous work, in which high TOF value above 600 h^{-1} was achieved in Au/FeO_x-573 catalyst [36].

5. Conclusions

The iron oxides with different crystal phases obtained from commercial source are used as support for gold catalysts. Factors influencing the activity including support morphology and porosity can be ruled out because the physico-chemical properties of the oxides are very similar. The catalytic activity results show that the selective oxidation of 1,4-butanediol to γ-butyrolactone is highly sensitive toward both the microcrystalline structure and the oxidation state of the iron oxide. The TOF value in the initial period follows the order Au/Fe_3O_4 > Au/α-Fe_2O_3 > Au/γ-Fe_2O_3, but the highest conversion and yield is obtained on Au/α-Fe_2O_3. Gold particle size in Au/Fe_3O_4 catalysts can be adjusted by using different pretreatment atmospheres. Activity tests indicate that the higher reaction rate of the catalyst with smaller gold particles is due to the increase in gold dispersion and the consequent high surface gold concentration. Variation of activity in Au/Fe_3O_4–Ar, Au/α-Fe_2O_3, and Au/γ-Fe_2O_3 is ascribed to the deviation in the intrinsic properties of the iron oxide that would cause changes in gold geometry, gold oxidation state, and gold-support contact structures. The support effect is more important in the present reaction system than the gold size effect.

Acknowledgments

This work was financially supported by the Major State Basic Resource Development Program (Grant No. 2003CB615807), NSFC (Project 20573024), and Science and Technology Commission of Shanghai Municipality (08DZ2270500, 06JC14004).

References

[1] M. Haruta, N. Yamada, T. Kobayashi, S. Iijima, J. Catal. 115 (1989) 301.
[2] D. Andreeva, V. Idakiev, T. Tabakova, A. Andreev, J. Catal. 158 (1996) 354.
[3] D. Andreeva, V. Idakiev, T. Tabakova, A. Andreev, R. Giovanoli, Appl. Catal. A 134 (1996) 275.
[4] A. Abad, P. Concepción, A. Corma, H. García, Angew. Chem. Int. Ed. 44 (2005) 4066.
[5] W.C. Ketchie, Y.L. Fang, M.S. Wong, M. Murayama, R.J. Davis, J. Catal. 250 (2007) 94.
[6] M. Comotti, C.D. Pina, R. Matarrese, M. Rossi, A. Siani, Appl. Catal. A 291 (2005) 204.
[7] T. Hayashi, K. Tanaka, M. Haruta, J. Catal. 178 (1998) 566.
[8] M.D. Hughes, Y.J. Xu, P. Jenkins, P. McMorn, P. Landon, D.I. Enache, A.F. Carley, G.A. Attard, G.J. Hutchings, F. King, E.H. Stitt, P. Johnston, K. Griffin, C.J. Kiely, Nature 437 (2005) 1132.
[9] B.E. Solsona, T. Garcia, C. Jones, S.H. Taylor, A.F. Carley, G.J. Hutchings, Appl. Catal. A 312 (2006) 67.
[10] M.A. Centeno, M. Paulis, M. Montes, J.A. Odriozola, Appl. Catal. A 234 (2002) 65.
[11] C. Milone, R. Ingoglia, L. Schipilliti, C. Crisafulli, G. Neri, S. Galvagno, J. Catal. 236 (2005) 80.
[12] J. Jia, K. Haraki, J.N. Kondo, K. Domen, K. Tamaru, J. Phys. Chem. B 104 (2000) 11153.
[13] M. Haruta, S. Tsubota, T. Kobayashi, H. Kageyama, M.J. Genet, B. Delmon, J. Catal. 144 (1993) 175.
[14] J. Guzman, B.C. Gates, J. Am. Chem. Soc. 126 (2004) 2672.
[15] D.A.H. Cunningham, W. Vogel, H. Kageyama, S. Tsubota, M. Haruta, J. Catal. 177 (1998) 1.
[16] M. Daté, M. Okumura, S. Tsubota, M. Haruta, Angew. Chem. Int. Ed. 43 (2004) 2129.
[17] M.M. Schubert, S. Hackenberg, A.C. van Veen, M. Muhler, V. Plzak, R.J. Behm, J. Catal. 197 (2001) 113.
[18] A.C. Gluhoi, N. Bogdanchikova, B.E. Nieuwenhuys, J. Catal. 229 (2005) 154.
[19] M. Comotti, W.C. Li, B. Spliethoff, F. Schuth, J. Am. Chem. Soc. 128 (2006) 917.
[20] H.H. Kung, M.C. Kung, C.K. Costello, J. Catal. 216 (2003) 425.
[21] W. Yan, S. Brown, Z. Pan, S.M. Mahurin, S.H. Overbury, S. Dai, Angew. Chem. Int. Ed. 45 (2006) 3614.
[22] P. Nopphawan, Z. Zhong, J. Guo, Y.F. Han, T.J. White, Gold Bull. 41 (2008) 42.
[23] S. Carrettin, Y. Hao, V. Aguilar-Guerrero, B.C. Gates, S. Trasobares, J.J. Calvino, A. Corma, Chem. Eur. J. 13 (2007) 7771.
[24] K. Qian, W. Huang, Z. Jiang, H. Sun, J. Catal. 248 (2007) 137.
[25] A.C. Gluhoi, N. Bogdanchikova, B.E. Nieuwenhuys, J. Catal. 232 (2005) 96.
[26] W. Yan, S.M. Mahurin, Z. Pan, S.H. Overbury, S. Dai, J. Am. Chem. Soc. 127 (2005) 10480.
[27] X. Zhang, H. Wang, B.Q. Xu, J. Phys. Chem. B 109 (2005) 9678.
[28] V. Idakiev, T. Tabakova, A. Naydenov, Z.Y. Yuan, B.L. Su, Appl. Catal. B: Environ. 63 (2006) 178.
[29] Y.F. Han, Z. Zhong, K. Ramesh, F. Chen, L. Chen, J. Phys. Chem. C 111 (2007) 3163.
[30] R. Si, M. Flytzani-Stephanopoulos, Angew. Chem. Int. Ed. 47 (2008) 2884.
[31] X. Bokhimi, R. Zanella, J. Phys. Chem. C 111 (2007) 2525.
[32] W. Yan, B. Chen, S.M. Mahurin, V. Schwartz, D.R. Mullins, A.R. Lupini, S.J. Pennycook, S. Dai, S.H. Overbury, J. Phys. Chem. B 109 (2005) 10676.
[33] K.Y. Ho, K.L. Yeung, Gold Bull. 40 (2007) 15.
[34] W. Yan, B. Chen, S.M. Mahurin, S. Dai, S.H. Overbury, Chem. Commun. (2004) 1918.
[35] J. Li, J. Chen, W. Song, J. Liu, W. Shen, Appl. Catal. A 334 (2008) 321.
[36] J. Huang, W.L. Dai, K. Fan, J. Phys. Chem. C 112 (2008) 16110.
[37] Y. Sasaki, Electrochemistry 76 (2008) 2.
[38] A.C. Albertsson, I.K. Varma, Biomacromolecules 4 (2003) 1466.
[39] F. Moreau, G.C. Bond, Catal. Today 122 (2007) 215.
[40] J. Hua, Q. Zheng, Y. Zheng, K. Wei, X. Lin, Catal. Lett. 102 (2005) 99.
[41] A.M. Visco, F. Neri, G. Neri, A. Donato, C. Milone, S. Galvagno, Phys. Chem. Chem. Phys. 1 (1999) 2869.
[42] J. Huang, W.L. Dai, H. Li, K. Fan, J. Catal. 252 (2007) 69.
[43] C. Milone, C. Crisafulli, R. Ingoglia, L. Schipilliti, S. Galvagno, Catal. Today 122 (2007) 341.
[44] S. Scir, S. Minic, C. Crisafulli, S. Galvagno, Catal. Commun. 2 (2001) 229.
[45] S.E. Collins, J.M. Cies, E. delRio, M. Lopez-Haro, S. Trasobares, J.J. Calvino, J.M. Pintado, S. Bernal, J. Phys. Chem. C 111 (2007) 14371.
[46] A.A. Herzing, C.J. Kiely, A.F. Carley, P. Landon, G.J. Hutchings, Science 321 (2008) 1331.